
A HYBRID ALGORITHM OF FAST INVARIANT IMBEDDING AND DOUBLING-ADDING METHODS FOR EFFICIENT MULTIPLE SCATTERING CALCULATIONS

Kiyoshi Kawabata

Department of Physics, College of Science, Tokyo University of Science, Shinjuku-ku, Tokyo 162-8601, Japan
E-mail address : kawabata@rs.kagu.tus.ac.jp

ABSTRACT

An efficient hybrid numerical method for multiple scattering calculations is proposed. We use the well established doubling–adding method to find the reflection function of the lowermost homogeneous slab comprising the atmosphere of our interest. This reflection function provides the initial value for the fast invariant imbedding method of Sato *et al.* (1977), with which layers are added until the final reflection function of the entire atmosphere is obtained. The execution speed of this hybrid method is no slower than one half of that of the doubling–adding method, probably the fastest algorithm available, even in the most unsuitable cases for the fast invariant imbedding method. The efficiency of the proposed method increases rapidly with the number of atmospheric slabs and the optical thickness of each slab. For some cases, its execution speed is approximately four times faster than the doubling–adding method.

Subject headings: multiple scattering, radiative transfer, invariant imbedding, doubling–adding, hybrid method

1. Introduction

Accurate and sufficiently rapid multiple scattering calculations of the intensity distributions of solar radiation reflected by planetary atmospheres are essential for performing the terrestrial and planetary remote sensing studies. Many methods for performing multiple scattering calculations have been proposed (e.g., Hansen and Travis, 1974; Natsuyama *et al.* 1998; Liou, 2002; Hovenier *et al.* 2004; Mishchenko *et al.* 2006). The *invariant imbedding* method is one such method, and it derives a set of integro-differential equations for reflection and transmission functions. It yields these equations by considering the change in the intensity of outgoing radiation when a very thin slab with given optical properties is added either to the top or bottom of the main body of the at-

mosphere. Although the equations thus derived are the same as those derived by Chandrasekhar (1960) by means of the invariance principle, the invariant imbedding method provides us with a short cut to arrive at them; therefore we call them *invariant imbedding equations*.

The *doubling* method, in contrast to the invariant imbedding method, finds reflection and transmission functions for a stack of two identical homogeneous layers whose reflection and transmission functions are known. First, a slab of sufficiently small optical thickness is considered, so that its reflection and transmission functions can be well approximated by single and second-order scattering solutions, which are simple. By repeating this doubling procedure, the reflection and transmission functions of any homogeneous atmosphere of arbitrary optical thickness can be pro-

duced. Note that the doubling method is a special case of the *adding* method, where the reflection and transmission functions of a stack of two slabs of different optical properties are sought.

One important problem associated with solving the invariant imbedding equations is that they belong to a class of so-called *stiff differential equations*. Therefore, it is extremely difficult to numerically integrate them with any standard technique such as the Runge–Kutta method even with an extremely small step size.

The *fast invariant imbedding* method of Sato *et al.* (1977) circumvents this problem by approximating the source term of each equation by low order polynomials of optical height τ measured upward from the ground surface. This approximation is initially a linear function followed by a piecewise quadratic polynomial of τ . These equations are then integrated semianalytically over τ . As a result, we obtain a set of nonlinear implicit equations for the reflection and transmission functions at each integration step. These equations can then be solved directly by successive iterations.

However, the fast invariant imbedding method still tends to be several times slower than the doubling–adding method for atmospheres of moderate or large optical thickness. In this study, we therefore attempt to improve the computational efficiency of the fast invariant imbedding method by incorporating the doubling–adding method to initialize the reflection and transmission functions of the lowermost layer.

2. Formulations

2.1. Basic Equations

For simplicity, we ignore the effect of polarization of radiation, so that the scalar approximation of the relevant quantities is valid. Let us also restrict our argument primarily to the computational aspect of the reflection function in view of remote sensing applications. Furthermore, we assume that the entire atmosphere of optical thickness τ_T is suitably approximated by N homogeneous slabs, with the first slab being the lowermost, and the N -th slab being the topmost as in Kawabata and Hirata (1985). In addition, we assume that the ground acts like a Lambert surface of reflectivity A_{grd} , which isotropically reflects in-

cident light.

Let us measure the optical height τ of a given location from the ground, because we intend to build the atmospheres of interest by stacking slabs upward. Furthermore, let $\Delta\tau_n$ denote the optical thickness of the n -th slab. Then, the total optical height $\tau_{\text{tot},n}$ of the upper surface of the n -th slab is given by

$$\tau_{\text{tot},n} = \sum_{j=1}^n \Delta\tau_j. \quad (1)$$

Hence, $\tau_{\text{tot},N} = \tau_T$, i.e., the total optical thickness of the entire atmosphere as shown in Fig. 1.

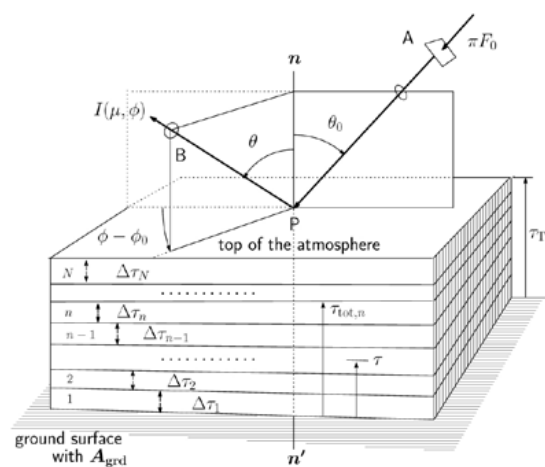


Fig. 1.— Geometry for multiple scattering calculations. The incident light with flux πF_0 per unit area (designated by A) perpendicular to the direction of incidence given by the zenith angle θ_0 and the azimuth angle ϕ_0 enters a point P on the top of the atmosphere, and emerges with the intensity $I(\mu, \phi)$ in the direction B specified by the zenith angle θ and the azimuth angle ϕ . The atmosphere is plane-parallel and scattering–absorbing, and it has total optical thickness τ_T . The zenith angles θ and θ_0 are measured from the local upward normal \mathbf{n} , and the azimuth angles ϕ and ϕ_0 are measured counterclockwise when the upper surface of the atmosphere is observed from above. The atmosphere is assumed to be stratified with N homogeneous slabs of optical thickness $\Delta\tau_n$ ($n = 1, 2, \dots, N$), and it is bounded at its bottom by a Lambert surface having reflectivity A_{grd} . The straight line \mathbf{n}' indicates the downward normal perpendicular to the bottom surface.

The intensity $I(\mu, \phi)$ of radiation reflected from a plane-parallel atmosphere can be specified by zenith and azimuth angles. The zenith angles θ and θ_0 measure the radiation emergence and incidence directions, respectively, with respect to the outward normal \mathbf{n} to the upper surface of the atmosphere in question. The azimuth angles ϕ and ϕ_0 for these two directions, respectively, are measured counterclockwise when the upper surface is observed from above.

For a monodirectional light incident from a direction (μ_0, ϕ_0) , the intensity of reflected light $I(\mu, \phi)$ emerging from the atmosphere in the direction (μ, ϕ) measured with respect to the upward normal \mathbf{n} to the topmost surface (Fig. 1) can be expressed in terms of the reflection function $R(\tau; \mu, \mu_0, \phi - \phi_0)$ as (e.g., Hansen and Travis, 1974)

$$I(\mu, \phi) = R(\tau_T; \mu, \mu_0, \phi - \phi_0) \mu_0 F_0 \quad (0 \leq \mu, \mu_0 \leq 1), \quad (2)$$

where F_0 is the radiation flux in units of π flowing per unit time through a unit area perpendicular to the direction of incidence, $\mu = \cos \theta$, and $\mu_0 = \cos \theta_0$. The zenith angles θ and θ_0 range from 0° to 90° and are measured with respect to the outward normal to the upper surface of the atmosphere \mathbf{n} . (The transmission function $T(\tau_T; \mu, \mu_0, \phi - \phi_0)$ can be similarly defined, but it is not restated here.)

To reduce the computational burden, let us expand the reflection function as well as other related quantities by using a Fourier series of $\phi - \phi_0$, such that

$$R(\tau; \mu, \mu_0, \phi - \phi_0) = \sum_{m=0}^M (2 - \delta_{m0}) R^m(\tau; \mu, \mu_0) \times \cos m(\phi - \phi_0), \quad (3)$$

where δ_{0m} designates the Kronecker delta. The Fourier coefficient of the reflection function $R^m(\tau; \mu, \mu_0)$ then satisfies the following invariant imbedding equation (Sato *et al.* 1977) :

$$\frac{\partial R^m(\tau; \mu, \mu_0)}{\partial \tau} = - \left(\frac{1}{\mu} + \frac{1}{\mu_0} \right) R^m(\tau; \mu, \mu_0) + S^m(\tau; \mu, \mu_0), \quad (4)$$

where the source function $S^m(\tau; \mu, \mu_0)$ is defined

as

$$S^m(\tau; \mu, \mu_0) = \frac{1}{4\mu\mu_0} P^m(\tau; -\mu, \mu_0) + \frac{1}{2\mu} \int_0^1 P^m(\tau; \mu, \mu') R^m(\tau; \mu', \mu_0) d\mu' + \frac{1}{2\mu_0} \int_0^1 R^m(\tau; \mu, \mu') P^m(\tau; \mu', \mu_0) d\mu' + \int_0^1 R^m(\tau; \mu, \mu') \left[\int_0^1 P^m(\tau; -\mu', \mu'') \times R^m(\tau; \mu'', \mu_0) d\mu'' \right] d\mu', \quad (5)$$

together with the initial condition given at the ground surface by

$$R^m(0; \mu, \mu_0) = A_{\text{grd}} \delta_{m0} \quad (0 \leq A_{\text{grd}} \leq 1). \quad (6)$$

The functions $P^m(\tau; -\mu, \mu_0)$ and $P^m(\tau; \mu, \mu_0)$ in Eq.(5) are the Fourier coefficients of the mean phase function at the optical height τ which include the effect of the single scattering albedo of each scattering agent present therein :

$$P^m(\tau; u, u_0) = \sum_{k=0}^{K_s} \varpi_{0,k}(\tau) \xi_k(\tau) P_k^m(\tau; u, u_0) \quad (-1 \leq u, u_0 \leq 1). \quad (7)$$

Note that $k = 0$ corresponds to atmospheric molecules causing Rayleigh scattering, whereas $k \geq 1$ corresponds to aerosols. Also note that we have employed the notations $u = \cos \vartheta$ and $u_0 = \cos \vartheta_0$ defined with nadir angles ϑ and ϑ_0 , both ranging from 0° to 180° with respect to the downward normal \mathbf{n}' (Fig. 1). The quantity $\varpi_{0,k}(\tau)$ is the single scattering albedo of the k -th type scattering-absorbing agent located at a given optical height τ , and $\xi_k(\tau)$ is its fractional contribution to the total extinction coefficient per unit volume of the atmosphere there :

$$\varpi_{0,k}(\tau) = \sigma_{s,k}(\tau) / [\sigma_{s,k}(\tau) + \sigma_{a,k}(\tau)] \quad (8a)$$

$$\xi_k(\tau) = \frac{\sigma_{s,k}(\tau)}{\varpi_{0,k}(\tau)} n_k(\tau) / \sum_{j=0}^{K_s} \frac{\sigma_{s,j}(\tau)}{\varpi_{0,j}(\tau)} n_j(\tau) \quad (8b)$$

where $\sigma_{s,k}(\tau)$ and $\sigma_{a,k}(\tau)$ represent the scattering coefficient and the absorption coefficient per k -th type particle, respectively, and $n_k(\tau)$ represents the volume number density of the k -th type particles at τ . The Fourier coefficient of the phase

function for the k -th type particles $P_k^m(\tau; u, u_0)$ in Eq.(7) is given by

$$P_k^m(\tau; u, u_0) = \frac{1}{\pi} \int_0^\pi P_k[\tau; \Theta(u, u_0, \phi - \phi')] \times \cos(\phi' - \phi_0) d\phi', \quad (9)$$

where Θ is the scattering angle specified by

$$\cos \Theta(u, u_0, \phi - \phi_0) = uu_0 + \sqrt{(1 - u^2)(1 - u_0^2)} \times \cos(\phi - \phi_0). \quad (10)$$

Because each of the N slabs comprising the atmosphere is assumed to be homogeneous, these τ -dependent quantities can be kept constant within a given slab.

To obtain the numerical solution of Eq.(4), we discretize it using the N_θ -th order Gauss–Legendre quadrature points and their corresponding weights for performing the numerical integrations over μ' and μ'' . The solutions for $R^m(\tau_T; \mu, \mu_0)$ are then generated at the mesh points specified by the quadrature points on a square matrix of size unity. To these, we may also add a certain number (N_{ext}) of non-quadrature μ -points for the convenience of interpolations of $R^m(\tau_T; \mu, \mu_0)$ tables to obtain the emergent intensity of reflected light, $I(\mu, \phi)$, for a given angular set of $(\mu, \mu_0, \phi - \phi_0)$.

2.2. Fast Invariant Imbedding Method

By introducing a new variable t defined as

$$t = \tau - \tau_{\text{tot}, n-1}, \quad (11)$$

to specify the given optical height τ in terms of the height measured from the bottom of each slab, Eq.(4) can be written in the short hand notation as

$$\frac{\partial R(t + \tau_{\text{tot}, n-1})}{\partial t} = -CR(t + \tau_{\text{tot}, n-1}) + S(t + \tau_{\text{tot}, n-1}), \quad (12)$$

where the constant C denotes $1/\mu + 1/\mu_0$, and the index n indicates the process of finding the solution for an atmosphere consisting of the first n slabs. Note that for large values of C , corresponding to a highly slanted incident or emergent radiation, this equation becomes *stiff* (see, e.g., Press *et al.* 1992 for a detailed discussion). Therefore,

obtaining the solution with sufficient accuracy requires some elaborate numerical tactics. In the remaining sections, we shall delineate our method.

Given the value of $R(t_j + \tau_{\text{tot}, n-1})$ at the j -th division point t_j within the n -th slab, the solution at the next step t_{j+1} , i.e., $R(t_{j+1} + \tau_{\text{tot}, n-1})$, is given by

$$R(t_{j+1} + \tau_{\text{tot}, n-1}) = R(t_j + \tau_{\text{tot}, n-1}) \exp[-C \cdot (t_{j+1} - t_j)] + \int_{t_j}^{t_{j+1}} S(t + \tau_{\text{tot}, n-1}) \exp[-C(t_{j+1} - t)] dt \quad (13)$$

with $t_1 = 0$. This equation should be used recursively until the solution $R(\tau_{\text{tot}, n})$ is obtained. The initial condition at t_1 is equal to the solution of an atmosphere having $(n - 1)$ -slabs, i.e., $R(t_1 + \tau_{\text{tot}, n-1}) = R(\tau_{\text{tot}, n-1})$.

(i) Solution at t_2 ($j = 1$):

The source function $S(t + \tau_{\text{tot}, n-1})$ is approximated by the first-order Lagrange polynomial of t passing through two points $(t_1, S(t_1 + \tau_{\text{tot}, n-1}))$ and $(t_2, S(t_2 + \tau_{\text{tot}, n-1}))$ as

$$S(t + \tau_{\text{tot}, n-1}) = \frac{1}{t_{21}} \{-S(t_1 + \tau_{\text{tot}, n-1}) \times (t - t_2) + S(t_2 + \tau_{\text{tot}, n-1})(t - t_1)\} \quad (14)$$

with $t_{21} \equiv t_2 - t_1$.

Substituting Eq.(14) into Eq.(13) with $j = 1$ and analytically integrating over t , we obtain

$$R(t_2 + \tau_{\text{tot}, n-1}) = F_a + F_b \cdot S(t_2 + \tau_{\text{tot}, n-1}) \quad (15)$$

where

$$F_a = R(t_1 + \tau_{\text{tot}, n-1})E_{21} + \frac{1}{C} (f_{21} - E_{21}) S(t_1 + \tau_{\text{tot}, n-1}), \quad (16a)$$

$$F_b = \frac{1}{C} (1 - f_{21}), \quad (16b)$$

$$f_{21} = \frac{1}{C\tau_{21}} (1 - E_{21}), \quad (16c)$$

$$E_{21} = \exp(-Ct_{21}). \quad (16d)$$

Although the value of F_a is already known, $S(t_2 + \tau_{\text{tot}, n-1})$ involves the unknown $R(t_2 + \tau_{\text{tot}, n-1})$. Hence, Eq.(15) is a nonlinear implicit equation for $R(t_2 + \tau_{\text{tot}, n-1})$, which is solved by

successive iterations starting with an obtained approximation, e.g., by setting $S(t_2 + \tau_{\text{tot},n-1}) = S(t_1 + \tau_{\text{tot},n-1})$, i.e.,

$$R(t_2 + \tau_{\text{tot},n-1}) = R(t_1 + \tau_{\text{tot},n-1}) \times \exp(-Ct_{21}) + t_{21}f_{21} \cdot S(t_1 + \tau_{\text{tot},n-1}). \quad (17)$$

The iterations are terminated when the condition

$$\text{Max.} \left| 1 - \frac{R^{\text{old}}(t_2 + \tau_{\text{tot},n-1})}{R^{\text{new}}(t_2 + \tau_{\text{tot},n-1})} \right| \leq \varepsilon_1 \quad (18)$$

is satisfied for every combination of μ - and μ_0 -quadrature points, where ε_1 designates the prescribed maximum relative error.

(ii) Solution at t_3 ($j=2$):

To increase the efficiency of integration over t , we take the step size that is larger than t_{21} by a factor α_1 (> 1), to obtain

$$t_3 = t_2 + \alpha_1 t_{21} = (1 + \alpha_1) t_{21} \quad (> 2 t_{21}). \quad (19)$$

The source function $S(t + \tau_{\text{tot},n-1})$ is approximated with the quadratic Lagrange polynomial of t that passes through the three points $(t_1, R(t_1 + \tau_{\text{tot},n-1}))$, $(t_2, R(t_2 + \tau_{\text{tot},n-1}))$, and $(t_3, R(t_3 + \tau_{\text{tot},n-1}))$, viz.,

$$\begin{aligned} S(t + \tau_{\text{tot},n-1}) &= S(t_1 + \tau_{\text{tot},n-1}) \cdot (t - t_2)(t - t_3)/(t_{21}t_{31}) - \\ &- S(t_2 + \tau_{\text{tot},n-1}) \cdot (t - t_3)(t - t_1)/(t_{21}t_{32}) + \\ &+ S(t_3 + \tau_{\text{tot},n-1}) \cdot (t - t_1)(t - t_2)/(t_{31}t_{32}), \quad (20) \end{aligned}$$

where we have set $t_{21} = t_2 - t_1$, $t_{31} = t_3 - t_1$, and $t_{32} = t_3 - t_2$.

Note that the values of $S(t_1 + \tau_{\text{tot},n-1})$ and $S(t_2 + \tau_{\text{tot},n-1})$ are now explicitly known. Substitution of Eq.(20) into Eq.(13), again upon analytical integration over t , yields

$$R(t_3 + \tau_{\text{tot},n-1}) = F_a + F_b \cdot S(t_3 + \tau_{\text{tot},n-1}), \quad (21)$$

where

$$\begin{aligned} F_a &= R(t_2 + \tau_{\text{tot},n-1}) \exp(-Ct_{32}) + \\ &+ H_1 \cdot S(t_1 + \tau_{\text{tot},n-1}) + \\ &+ H_2 \cdot S(t_2 + \tau_{\text{tot},n-1}), \quad (22a) \end{aligned}$$

$$\begin{aligned} F_b &= (2f_{32} + E_{32}t_{21} - (t_{31} + t_{32}) + \\ &+ Ct_{31}t_{32})/(C^2t_{31}t_{32}), \quad (22b) \end{aligned}$$

$$H_1 = (2f_{32} - (1 + E_{32})t_{32})/(C^2t_{21}t_{31}), \quad (22c)$$

$$\begin{aligned} H_2 &= (-2f_{32} + t_{31} + (t_{32} - t_{21} - \\ &- Ct_{21}t_{32})E_{32})/(C^2t_{21}t_{32}), \quad (22d) \end{aligned}$$

$$f_{32} = (1 - E_{32})/C, \quad (22e)$$

$$E_{32} = \exp(-Ct_{32}). \quad (22f)$$

Because $S(t_3 + \tau_{\text{tot},n-1})$ is a function of unknown $R(t_3 + \tau_{\text{tot},n-1})$, Eq.(21) is also a nonlinear implicit equation for $R(t_3 + \tau_{\text{tot},n-1})$. Therefore, we solve for $R(t_3 + \tau_{\text{tot},n-1})$ by successive iterations starting with an initial approximation given by a linear extrapolation of $R(t_1 + \tau_{\text{tot},n-1})$ and $R(t_2 + \tau_{\text{tot},n-1})$:

$$\begin{aligned} R(t_3 + \tau_{\text{tot},n-1}) &= \{(t_3 - t_1)R(t_2 + \tau_{\text{tot},n-1}) - \\ &- (t_3 - t_2)R(t_1 + \tau_{\text{tot},n-1})\}/t_{21}. \quad (23) \end{aligned}$$

The iterations are terminated as soon as the condition

$$\text{Max.} \left| 1 - \frac{R^{\text{old}}(t_3 + \tau_{\text{tot},n-1})}{R^{\text{new}}(t_3 + \tau_{\text{tot},n-1})} \right| \leq \varepsilon_1 \quad (24)$$

is fulfilled similar to procedure (i).

(iii) Solution at t_4 and above ($j \geq 3$):

To obtain $R(t_4 + \tau_{\text{tot},n-1})$, for instance, we first relocate the foregoing solutions and related quantities such that

$$\begin{aligned} t_2, R(t_2 + \tau_{\text{tot},n-1}), S(t_2 + \tau_{\text{tot},n-1}) &\Rightarrow \tau_1, R(t_1 + \tau_{\text{tot},n-1}), S(t_1 + \tau_{\text{tot},n-1}), \\ t_3, R(t_3 + \tau_{\text{tot},n-1}), S(t_3 + \tau_{\text{tot},n-1}) &\Rightarrow t_2, R(t_2 + \tau_{\text{tot},n-1}), S(t_2 + \tau_{\text{tot},n-1}). \end{aligned}$$

Then, we employ $t_3 + \alpha_1 t_{32}$ as a new value for t_3 and return to procedure (ii). From this process, the new solution is always obtained as $R(t_3 + \tau_{\text{tot},n-1})$. The process is repeated until $t_3 = \Delta\tau_n$ is attained.

If, however, the successive approximation for the solution at any step does not converge within a prescribed number of iterations N_{iter} , the integration step size must be reduced by a certain factor α_2 (< 1) before renewing the iteration.

Furthermore, the integration of Eq.(12) over t may be terminated whenever the maximum absolute value of the derivatives of $R(t + \tau_{\text{tot},n-1})$ with

respect to t falls below a preset value ε_2 :

$$\begin{aligned} & \text{Max.} |\partial R(t + \tau_{\text{tot},n-1})/\partial t| \\ & = \text{Max.} |-CR(t + \tau_{\text{tot},n-1}) + \\ & \quad + S(t + \tau_{\text{tot},n-1})| \leq \varepsilon_2 \end{aligned} \quad (25)$$

2.3. Doubling–Adding Method

We implement the doubling-adding method to determine reflection function for the lowermost slab of the atmosphere of interest to improve the computational efficiency.

Assume that the reflection and transmission functions for a homogeneous layer of optical thickness τ are known. Then we can obtain the reflection and transmission functions of a homogeneous layer of the same optical properties but of optical thickness 2τ by using equations of the doubling method (e.g., Hansen and Travis, 1974):

$$\begin{aligned} R^m(2\tau; \mu, \mu_0) &= R^m(\tau; \mu, \mu_0) + \\ & \quad + \exp(-\tau/\mu)U(\mu, \mu_0) + \\ & \quad + 2 \int_0^1 T^m(\tau; \mu, \mu')U(\mu', \mu_0)\mu' d\mu' \end{aligned} \quad (26a)$$

$$\begin{aligned} T^m(2\tau; \mu, \mu_0) &= \exp(-\tau/\mu)D(\mu, \mu_0) + \\ & \quad + T^m(\tau; \mu, \mu_0)\exp(-\tau/\mu_0) + \\ & \quad + 2 \int_0^1 T^m(\tau; \mu, \mu')D(\mu', \mu_0)\mu' d\mu' \end{aligned} \quad (26b)$$

where

$$Q_1(\mu, \mu_0) = 2 \int_0^1 R^m(\tau; \mu, \mu')R^m(\tau; \mu', \mu_0)\mu' d\mu', \quad (27a)$$

$$Q_n(\mu, \mu_0) = 2 \int_0^1 Q_1(\mu, \mu')Q_{n-1}(\mu', \mu_0)\mu' d\mu' \quad (n \geq 2), \quad (27b)$$

$$S(\mu, \mu_0) = \sum_{n=1}^{\infty} Q_n(\mu, \mu_0), \quad (27c)$$

$$\begin{aligned} D(\mu, \mu_0) &= T^m(\tau; \mu, \mu_0) + S(\mu, \mu_0)\exp(-\tau/\mu_0) + \\ & \quad + 2 \int_0^1 S(\mu, \mu')T^m(\tau; \mu', \mu_0)\mu' d\mu', \end{aligned} \quad (27d)$$

$$\begin{aligned} U(\mu, \mu_0) &= R^m(\tau; \mu, \mu_0)\exp(-\tau/\mu_0) + \\ & \quad + 2 \int_0^1 R^m(\tau; \mu, \mu')D(\mu', \mu_0)\mu' d\mu'. \end{aligned} \quad (27e)$$

We repeat the above procedure until the desired value of $\Delta\tau_1$ is reached. Note that the reflection and transmission functions thereby obtained do not consider the effect of ground reflectivity. If the atmosphere is bounded at its bottom by a Lambert surface of reflectivity A_{grd} , its effect manifests through the azimuth angle-independent Fourier coefficient $R^0(\Delta\tau_1; \mu, \mu_0)$, and the adding method gives rise to the following expression (p.64 of van de Hust, 1980) :

$$\begin{aligned} R_S^0(\Delta\tau_1; \mu, \mu_0) &= R^m(\Delta\tau_1; \mu, \mu_0) + \\ & \quad + \frac{A_{\text{grd}}}{1 - A_{\text{grd}}A_{\text{sph}}}t_a(\mu)t_a(\mu_0) \end{aligned} \quad (28)$$

where A_{sph} is the spherical or Bond albedo defined as

$$A_{\text{sph}} = 4 \int_0^1 \int_0^1 R^0(\Delta\tau_1; \mu, \mu_0)\mu\mu_0 d\mu d\mu_0, \quad (29)$$

and the function $t_a(\mu)$ is given by

$$t_a(\mu) = \exp(-\Delta\tau_1/\mu) + 2 \int_0^1 T^0(\Delta\tau_1; \mu, \mu')\mu' d\mu'. \quad (30)$$

To initialize the doubling calculation, we start with a slab of optical thickness τ_{in} given by

$$\tau_{\text{in}} = \Delta\tau_1/2^{N_0+N_D}, \quad (31)$$

where $N_0 = \text{int}\{\log_{10} \Delta\tau_1 / \log_{10} 2\}^1$, and N_D is a prescribed integer.

The reflection and transmission functions for this thickness are assumed to be sufficiently well approximated by the sum of the single and second-order scattering solutions (e.g., Kawabata and Ueno, 1988).

3. Multiple Scattering Calculations with Current Method

3.1. Setting up Numerical Calculations

Following Sato *et al.* (1977), we use the Venus cloud model of Hansen and Hovenier (1974) • •at

¹The symbol $\text{int}\{x\}$ used here signifies Gauss' symbol, i.e., the greatest integer that is equal to or less than x .

a wavelength 365 nm. This model was derived by them on the basis of a theoretical analysis of ground-based polarimetry data. Briefly, the cloud is a thick layer consisting of homogeneous mixture of CO₂ molecules and droplets of concentrated aqueous sulfuric acid that have a spherical shape. The real part of refractive index n_r of these droplets at this wavelength is assumed to be 1.46, and its imaginary part n_i is assumed to be 0. The size distribution of the radius r of the cloud particles is approximated by the gamma distribution characterized by an effective radius r_{eff} of 1.05 μm and an effective variance v_{eff} of 0.07:

$$n(r) = \frac{(ab)^{(2b-1)/b}}{\Gamma[(1-2b)/b]} r^{(1-3b)/b} \exp(-r/ab), \quad (32)$$

where $a = r_{\text{eff}}$, $b = v_{\text{eff}}$, and Γ is the gamma function (Hansen and Travis, 1974).

The phase function for the cloud particles averaged over this size distribution can be generated by a Mie scattering computer code.

However, the UV absorbers that are definitely present in the actual clouds are completely ignored in this study to maximize the effect of multiple scattering of light. Therefore, the single scattering albedos $\varpi_{0,k}$ ($k = 0, 1$), i.e., Eq.(8a), of the molecules and aerosol particles are set to be unity. The extinction fraction ξ_0 due to Rayleigh scattering by CO₂ molecules is assumed to be 0.04. Thus, the extinction fraction by sulfuric acid cloud particles ξ_1 is 0.96 (Eq.(8b)).

The optical thickness of the cloud layer is assumed to be 128 in the current study, and a Lambert surface with $A_{\text{grd}} = 1$ is placed at its bottom.

The Fourier sum indicated in Eq.(3) for $R(\tau; \mu, \mu_0, \phi - \phi_0)$ is terminated at $M = 34$, and a 150-point Gauss-Legendre quadrature is applied to integrate Eq.(9) over ϕ' to obtain the Fourier coefficients of the phase function.

A) Fast Invariant Imbedding Calculations

On the basis of various past experiments, we adopt the following values for the relevant parameters:

$$\begin{aligned} N_\theta &= 29, & N_{\text{iter}} &= 30, & \tau_{21} &= 10^{-2}, \\ \alpha_1 &= 1.2, & \alpha_2 &= 0.8, \\ \varepsilon_1 &= 10^{-8}, & \varepsilon_2 &= 10^{-10}. \end{aligned}$$

To choose a suitable value for N_θ (the order of the Gauss-Legendre quadrature for μ -integrations), we varied the value of N_θ in some

sample calculations of the intensity distribution $I(\mu, \phi)/F_0$ for the reflected sunlight along the intensity equator of a spherical planet viewed from an infinite distance with a phase angle of 5°. For this purpose, we first defined a Cartesian coordinate system on a projected planetary disk of unit radius such that the x -axis ran along the intensity equator and the y -axis ran perpendicular to it at the disk center which corresponds to the sub-observer point.

The scattering geometry at a given location (x, y) on the disk can then be specified by the following equations (e.g., Kawabata *et al.* 2000):

$$\mu = \sqrt{1 - (x^2 + y^2)}, \quad (33a)$$

$$\mu_0 = \mu \cos \alpha + x \sin \alpha, \quad (33b)$$

$$\cos(\phi - \phi_0) = (\mu\mu_0 - \cos \alpha)/A, \quad (33c)$$

$$\sin(\phi - \phi_0) = y \sin \alpha/A, \quad (33d)$$

$$A = \sqrt{(1 - \mu^2)(1 - \mu_0^2)}, \quad (33e)$$

where α is the phase angle.

The intensity equator corresponds to $y = 0$, and the sub-solar point is located at $(\sin \alpha, 0)$. The bright limb and the terminator of the planetary disk intersect with the x -axis at $(1, 0)$ and $(-\cos \alpha, 0)$, respectively, for positive values of α .

For the geometry $(\mu, \mu_0, \phi - \phi_0)$ associated with a given location $(x, 0)$, the square tables of the Fourier coefficient of the reflection function $R^m(\tau_\Gamma; \mu, \mu_0)$ are interpolated at (μ, μ_0) by using the bicubic interpolation method (Press *et al.* 1992). Then the results are summed up according to Eq.(3) to produce $R(\tau_\Gamma; \mu, \mu_0, \phi - \phi_0)\mu_0$, which is just equal to the emergent intensity $I(\mu, \phi)/F_0$ of the reflected sunlight at the point in question. Furthermore, we add two extra μ -points, viz., 0.1 and 1, to conveniently interpolate the R^m tables.

Fig. 2 shows three intensity distributions $I(\mu, \phi)/F_0$ calculated along the intensity equator for $N_\theta = 7, 15$, and 29 (only the portions with $I(\mu, \phi)/F_0 \geq 0.9$ are displayed). The model atmosphere employed for these calculations is the Hansen-Hovenier Venus cloud model consisting of CO₂ molecules and aerosol particles of concentrated sulfuric acid as described previously in this section.

Obviously, it is imperative that N_θ should be sufficiently large to obtain reliable theoretical intensity distributions. For this reason, we adopt

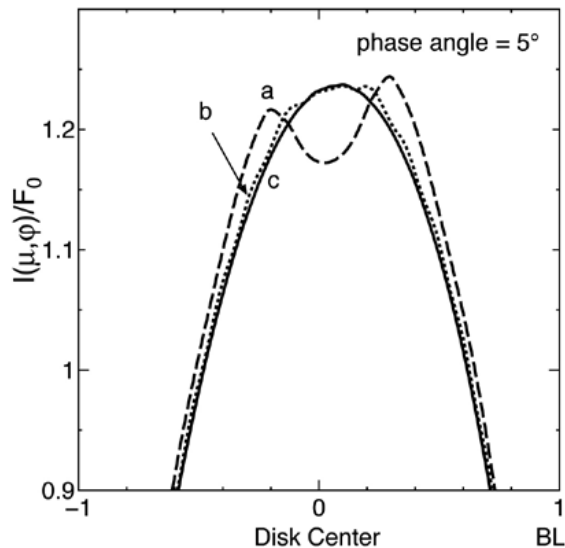


Fig. 2.— Calculated emergent intensity distributions along the intensity equator of a planetary disk. The curves a, b, and c are the theoretical distributions of the intensity $I(\mu, \phi)/F_0$ along the intensity equator of a spherical planet for a phase angle of 5° ; they were calculated adopting a Gauss–Legendre quadrature of $N_\theta = 7, 15,$ and $29,$ respectively. Note that F_0 is the flux of the incident radiation in units of π (only the portions with $I(\mu, \phi)/F_0 \geq 0.9$ are shown). The locations $x = 0$ and $1,$ respectively, correspond to the disk center (or sub-observer point) and the bright limb (BL). A Hansen–Hovenier Venus model cloud for a wavelength of 365 nm was employed, except that the single scattering albedo was set to unity, and the bottom was bounded by a perfectly reflecting Lambert surface, as described in the text.

$N_\theta = 29$ for subsequent multiple scattering calculations.

Note that obtaining the numerical solution of Eq.(12) by means of, e.g., the ordinary fourth-order Runge–Kutta method requires a step size t_{21} comparable to or much smaller than the minimal value of C^{-1} . With $N_\theta = 29,$ we would therefore have to employ a value less than or equal to 10^{-3} for t_{21} .

Furthermore, we must maintain $\alpha_1 = 1$ for the step size throughout the process of integration until the entire atmosphere is completed. In fact, the

CPU time required for the Runge–Kutta method to obtain $R^0(128; \mu, \mu_0)$ for the Hansen–Hovenier Venus model cloud of optical thickness 128 but with the unit single scattering albedo is found to be larger than that required by the fast invariant imbedding method by more than a factor of 900.

Therefore, it is impractical to employ the Runge–Kutta method as a numerical solver of the invariant imbedding equations.

B) Doubling–Adding Calculations

First of all, our current method requires the doubling–adding method to produce the reflection function for the lowermost slab of optical thickness $\Delta\tau_1,$ although the use of the adding method is rather implicit in this case due to the fact that a Lambert plane is assumed for the bottom surface. As in A), we employ $N_\theta = 29$ for the Gauss–Legendre quadrature to perform the μ -integrations involved in Eqs.(26) and (27).

To set up the value for $\tau_{in},$ we adopt $N_D = 25$ for Eq.(31), which implies that the starting solutions for the reflection and transmission functions $R^m(\tau_{in}; \mu, \mu_0)$ and $T^m(\tau_{in}; \mu, \mu_0),$ respectively, are generated for a homogeneous layer of an optical thickness of the order of $10^{-8},$ by summing the single and second-order scattering solutions using the expressions of Kawabata and Ueno (1988). For the Fourier summation of Eq. (3), $M = 34$ is adopted as is done for the fast invariant imbedding method.

Secondly, for comparison, we also perform the doubling–adding calculations with the same parameter values as indicated above employing the model atmospheres used to test the current method.

3.2. Numerical Comparison

The filled circles in Fig. 3 show the ratio of the CPU time required by the fast invariant imbedding method $t(\text{FII})$ to that required by the doubling–adding method $t(\text{DA})$ to obtain the first 35 Fourier coefficients $R^m(128; \mu, \mu_0)$ ($m = 0, 1, 2, \dots, 34$) for a conservatively scattering Hansen–Hovenier cloud. This ratio is presented as a function of the degree of the Gauss–Legendre quadrature $N_\theta.$ The cloud has an optical thickness of 128, and it is bounded by a perfect Lambert surface with $A_{\text{grd}} = 1$ at its bottom. The solid curve

is a cubic-polynomial least square fit to the data. In case of a single thick homogeneous atmosphere,

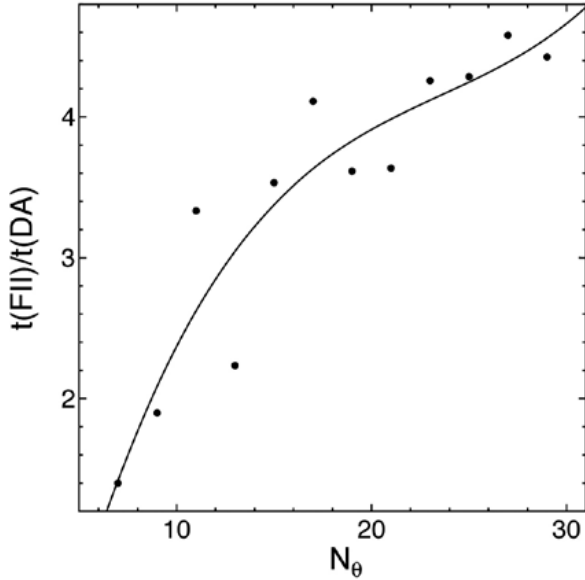


Fig. 3.— The CPU time $t(\text{FII})$ required for the fast invariant imbedding method to produce the reflection function $R(\tau_T; \mu, \mu_0, \phi - \phi_0)$ of the model atmosphere described in §3.1 compared to the doubling–adding method CPU time $t(\text{DA})$ as a function of the degree of the Gauss–Legendre quadrature, N_θ .

the CPU time of the fast invariant imbedding method rapidly increases with the value of N_θ : for $N_\theta = 29$, it is approximately five times slower than the doubling method. In other words, the fast invariant imbedding method can hardly compete with the doubling method for a single thick homogeneous atmosphere at high orders of the Gauss–Legendre quadrature.

Fig.4 shows, on the plane of the optical thickness of each slab τ_T/N versus the number of slabs N , a demarcation line along which the current hybrid method and the doubling–adding method work equally fast. Above this line (in the shaded area), the current hybrid method is faster than the doubling–adding method; below this line, the opposite is true. For a given number of slabs, all the slabs are set to equal optical thicknesses and optical properties identical to that of the Hansen–Hovenier Venus model cloud described in §3.1. The solid curve is a cubic–polynomial least square fit to the data. As the number of slabs increases,

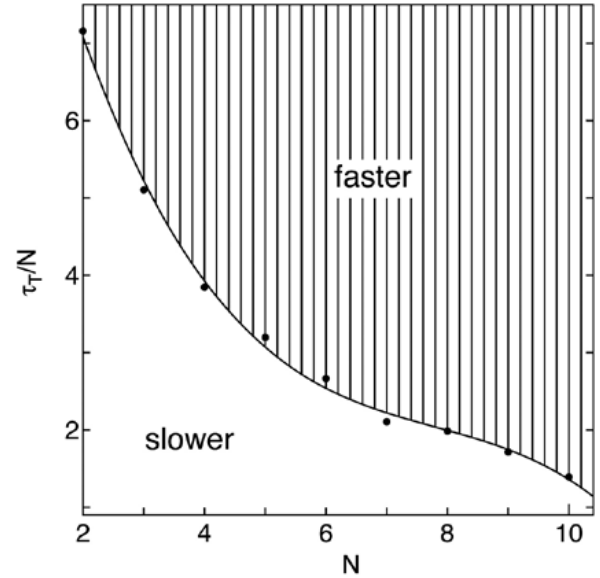


Fig. 4.— Demarcation line along which the current method works as fast as the doubling–adding method for τ_T/N (the optical thickness of each slab) versus N (the number of identical slabs comprising the atmosphere). The shaded area indicates the region where the hybrid method is faster than the doubling–adding method. The optical properties of each slab are those employed for Fig.3.

the efficiency of the current method increases, and the shaded area extends to an increasingly smaller optical thickness associated with each slab. This indicates that stacking up a large number of slabs by means of the current method is more rapid than by the doubling–adding method.

Fig. 5 shows the maximum value of the CPU time of the current method relative to the doubling–adding CPU time (left-hand side ordinate) as a function of the number of homogeneous slabs comprising an atmosphere whose optical properties are the same as those employed for Fig. 4. The filled circles are the data points, and the solid curve is a B-spline fit. The open circles are the data points for the right-hand side ordinate, which indicates the optical thickness of each slab that yields the maximum CPU time, and the dashed curve is a B-spline fit to them. • •

The column "current" in Table 1 shows a set

Table 1: Reflection function calculated by the current and doubling-adding methods

$R(\tau_T; \mu, \mu_0, \phi - \phi_0)\mu_0$	current	doub-add.
$R(35; 0.1, 0.1, 0^\circ) \times 0.1$	2.126698	2.126698
$R(35; 0.1, 0.1, 180^\circ) \times 0.1$	0.246565	0.246562
$R(35; 0.5, 0.5, 0^\circ) \times 0.5$	0.649196	0.649197
$R(35; 0.5, 0.5, 180^\circ) \times 0.5$	0.609809	0.609809
$R(35; 1.0, 1.0, 0^\circ)$	1.258023	1.257902

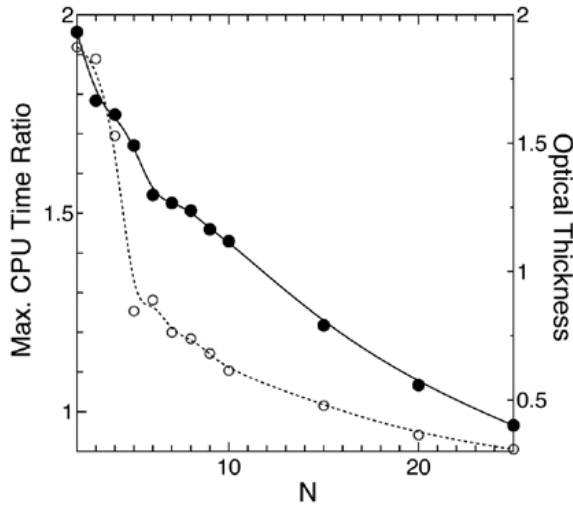


Fig. 5.— Maximum value of the CPU time required for the current method relative to the doubling-adding CPU time. The abscissa indicates the number of slabs of equal thickness comprising the atmosphere employed, and the left-hand side ordinate shows the maximum CPU time relative to the doubling-adding CPU time to perform the same set of multiple scattering calculations. The filled circles are the data points for the maximum CPU time ratio, and the solid curve is a B-spline fit to this data. The open circles are the data points for the optical thickness of each slab (refer to the right-hand side ordinate) that gives the maximum CPU time, and the dashed curve is a B-spline fit to this data. The optical properties of each slab are the same as those employed for Fig. 4.

of sample values of $R(35; \mu_0, \mu_0, \phi - \phi_0)\mu_0$ obtained by the current hybrid method for five combinations of $\mu_0 (= 0.1, 0.5, \text{ and } 1)$, and $\phi - \phi_0 (=$

0° and 180°). The model atmosphere employed is composed of seven identical slabs, each having an optical thickness of 5 and the same optical properties as those assumed for Fig. 4. The column "doub-add" shows the corresponding values of the reflection function produced by the doubling-adding method. Note that even the largest discrepancy found for $\mu_0 = 1$ is less than $10^{-2} \%$.

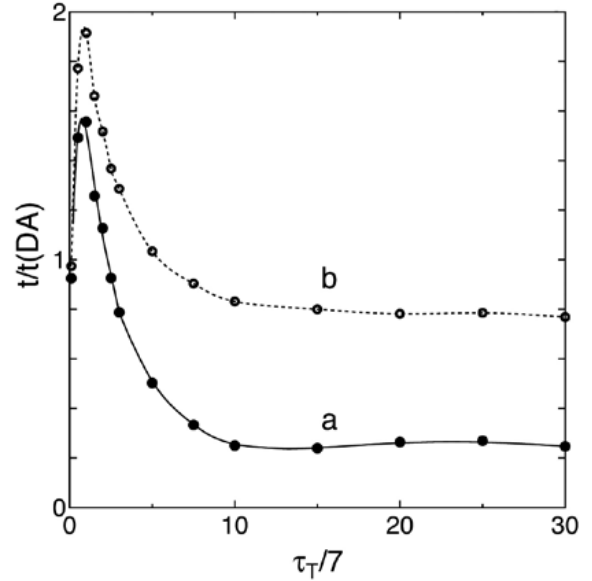


Fig. 6.— The CPU time of (a) the current hybrid method and (b) the fast invariant imbedding method compared to the doubling-adding method CPU time $t(\text{DA})$ for an atmosphere consisting of seven identical slabs as a function of the optical thickness $\tau_T/7$ of each slab. The current method is found to be significantly more efficient than the doubling-adding method for $\tau_T/7 \gtrsim 2.5$. In addition, note that the execution speed of the hybrid method is greater by almost a factor of four than the doubling-adding method for $\tau_T/7 \gtrsim 10$.

Fig. 6 shows the CPU time t of (a) the current hybrid method and (b) the fast invariant imbedding method compared to that of the doubling-adding method $t(\text{DA})$ for an atmosphere composed of seven identical slabs whose optical properties are the same as those for Fig. 4. The abscissa is the optical thickness of each slab $\tau_T/7 (= \Delta\tau_n, n = 1, 2, \dots, 7)$. The filled circles are the points for the current method, and the solid curve designated by the letter *a* is a B-spline curve fit to

them. The open circles are the data points for the fast invariant imbedding method, and the dashed curve designated by the letter *b* is a B-spline fit to them.

For $\tau_T/7 \gtrsim 2.5$, the hybrid method is definitely faster than the doubling–adding method and as the value of $\tau_T/7$ increases, the hybrid method’s CPU time asymptotically approaches approximately a quarter of that for the doubling–adding method. Although the opposite is the case for $\tau_T/7 \lesssim 2.5$, the relative CPU time of the current method is not greater than 1.6 occurring at $\tau_T/7 \simeq 0.7$.

In contrast, the relative CPU time of the fast invariant imbedding method is lower than that of the doubling–adding method only for $\tau_T/7 \gtrsim 6$ and approaches a limiting value of approximately 0.75 as $\tau_T/7$ increases. This limiting value is, however, almost a factor of three larger than that of the hybrid method. For optical thicknesses less than 6, the fast invariant imbedding method is slower than the doubling–adding method, and the relative CPU time is 1.92 at $\tau_T/7 = 1$ (as opposed to 1.6 at $\tau_T/7 = 0.7$ for the current method as stated above). These facts firmly attest to the high practicability of the current method as a computational tool for remote sensing data analyses.

Note that the results described above are for a stack of slabs of equal optical thickness. In actual model calculations, however, the lowermost slab is likely to have the largest optical thickness. Therefore, the efficiency of the current method in actual model calculations is higher than that observed in this section.

4. Conclusion

We have succeeded in creating a new and highly efficient method for multiple scattering calculations by coupling the fast invariant imbedding method with the doubling–adding method.

Our new hybrid method enhances the advantage of these two methods, while complementing their shortcomings. The fast invariant imbedding method is for atmospheres composed of a large number of slabs, but tends to be significantly slower for atmospheres comprising a small number of relatively thick slabs. In contrast, the speed of the doubling–adding method is slow for atmospheres composed of a large number of slabs, be-

cause the number of the time-consuming adding calculations increases.

The execution speed of the new method may still turn out to be slower than the doubling–adding method, probably the fastest method proposed so far, in handling atmospheres stratified with a relatively small number of homogeneous slabs. For example, for a two-slab atmosphere, this hybrid method is slower than the doubling–adding method for the optical thicknesses less than 7 as observed from Fig.4. Even so, the CPU time required is not more than twice that required by the doubling–adding method.

Furthermore, for a larger number of slabs, the differences are likely to be much less significant, as shown in Figs. 5 and 6. In fact, for $N \gtrsim 25$, the speed of the current method surpasses that of the doubling–adding method. In addition, for a given number of slabs, this hybrid method is capable of working approximately four times faster than the doubling–adding method if the optical thickness of each layer is larger than a certain threshold value, as can be observed from Figs. 4 and 6.

All comparisons in this study are based on a stratified atmosphere consisting of slabs of equal optical thickness. However, in actual models, the lowermost slab tends to have the largest optical thickness. Under such circumstances, the hybrid method proposed in this study should prove more advantageous than the doubling–adding method in performing multiple scattering calculations.

Acknowledgment The author is grateful to the late Prof. Sueo Ueno for having directed his attention to the theory of radiative transfer.

REFERENCES

- Chandrasekhar, S. 1960, *Radiative Transfer*, Dover Publications, Inc. (New York).
- Hansen, J.E., Hovenier, J.W. 1974, *J. Atmos. Sci.* 31, 1137-1160.
- Hansen, J.E., Travis, L.D. 1974, *Space Sci. Rev.* 16, 527-610.

- Hovenier, J.W., van der Mee, C., Domke, H. 2004, *Transfer of Polarized Light in Planetary Atmospheres*, Kluwer Academic Publisher (Dordrecht).
- Kawabata, K., Hirata, R. 1985, *Astrophys. Space Sci.* 109, 345-356.
- Kawabata, K., Sato, M., Travis, L.D. 2000, *Applied Math. Comp.* 116, 115-132.
- Kawabata, K., Ueno, S. 1988, *Astrophys. Space Sci.* 150, 327-344.
- Liou, K.N. 2002, *An Introduction to Atmospheric Radiation*, Academic Press (Reading, Massachusetts).
- Mishchenko, M.I., Travis, L.D., Lacis, A.A. 2006, *Multiple Scattering of Light by Particles: Radiative Transfer and Coherent Backscattering*, Cambridge University Press (Cambridge).
- Natsuyama, H.H., Ueno, S., Wang, A.P., 1998, *Terrestrial Radiative Transfer: Modeling, Computation, and Data Analysis*, Springer-Verlag (Tokyo).
- Press, W.H., Teukolsky, S.A., Vetterling, W.T., Flannery, B.P. 1992, *Numerical Recipes in FORTRAN*, 2nd edition, Cambridge University Press (New York).
- Sato, M., Kawabata, K., Hansen, J.E. 1977, *Astrophys. J.*, 216, 947-962.
- van de Hulst, H.C. 1980, *Multiple Light Scattering; Tables, Formulas, and Applications*, Vol.1 & 2, Academic Press (New York).